
# Pixel History for Advanced Camera for Surveys Wide Field Channel

David Borncamp, Norman Grogin,
Matthew Bourque and Sara Ogaz

June 16, 2017

## Abstract

Excess thermal energy present in a Charged Coupled Device (CCD) can result in additional electrical current. This excess charge is trapped within the silicon lattice structure of the CCD electronics. It can persist through multiple exposures and have an adverse effect on science performance of the detectors unless properly flagged and corrected for. The traditional way to correct for this extra charge is to take occasional long-exposure images with the camera shutter closed. These images, generally referred to as “dark” images, allow for the measurement of the thermal-electron contamination present in each pixel of the CCD lattice. This so-called “dark current” can then be subtracted from the science images by re-scaling the dark to the corresponding exposure times. Pixels that have signal above a certain threshold are traditionally marked as “hot” and flagged in the data quality array. Many users will discard these because of the extra current. However, these pixels may not be unusable because of an unreliable dark subtraction; if we find these pixels to be stable over an anneal period, we can properly subtract the charge and the extra Poisson noise from this dark current will be propagated into the error arrays. Here we present the results of a pixel history study that analyzes every individual pixel of the Hubble Space Telescope's (HST)

Advanced Camera for Surveys (ACS) Wide Field Channel (WFC) CCDs over time and allows pixels that were previously flagged as unuseable to be brought back into the science image as a reliable pixel.

# 1. Introduction

CCDs are one of the most common types of imagers for astronomical science, much work has gone into understanding the basic properties of these devices (Coe & Grogin 2014, Mutchler et al. 2004, Riess 2002 a & b, Cox et al. 2003). This report documents a new type of analysis where every pixel is studied individually to determine the stability and evolution over time of the dark current in that pixel. The results of this will eventually be propagated into and affect every ACS/WFC data product. This document seeks to explain the methods that were developed and implemented to assist in this investigation to allow for the possibility for this data to be used in other surveys. Due to the construction of this study, many other projects can be conducted with methods discussed in this report.

When observing with CCDs, there are several steps that go into properly calibrating the data to achieve the best possible result. One of the first and most important steps is to measure and correct for the thermally generated electric current trapped within the layers of the silicon lattice that makes up the detector as this energy, which is independent of the target, can have adverse effects on the science result. This extra dark current needs to be properly calibrated or appropriately flagged before astronomical analysis can occur.

## 1.1 Dark Current

Dark current is called “dark” because it is an unintended signal that is present even when there is no light entering the detector (i.e. the detector is dark). This current manifests itself as slightly higher pixel count rates than are actually received from external light sources. It is usually generated by thermally excited valence electrons in the substrate of the CCD that are able to jump into the conduction band and then collect in the electrical potential well of a given pixel. The spatial pattern can be a low quasi-uniform effect and its effects expected to increase linearly with time on ACS/WFC (Golimowski et al. 2011). The traditional way to correct for this unintentional charge is to take long (1000 second) exposures with the shutter closed and subtract the scaled image from all science frames. Due to the closed shutter, there are no external light sources, so we can therefore assume that no other charge is generated from outside the detector. This ensures that the dark image is a measurement of the intrinsic amount of energy trapped within the detector’s pixels. These dark images, can characterize the amount of energy inherently trapped within the silicon lattice that physically comprises a CCD. In most cases, this extra charge can simply be subtracted out of science images. However this is not always valid as the dark current may change rapidly for a given pixel, causing the dark rates for the subtracted dark image to be inaccurate.

As shown by previous studies, there are three main sources of the generation of dark current within a CCD: at the surface, depletion, and diffusion (Widenhorn et al. 2002). Since the ACS CCDs are buried channel devices operated in Multi-Pinned Phases (MPP) mode (Avila, 2017), which inverts the silicon surface to reduce the surface dark current, the surface dark is negligible and the remaining dark current must come from the either depletion or diffusion. The extra current is still significant enough to warrant tracking throughout the lifetime of ACS, which is the main subject of our study presented here but we examine the dark current from the perspective of stability of the thermally generated electrons.

### 1.2 Hot Pixels

CCDs have individual pixels that contain unintended charge traps, characterized by a local discrepancy relative to the rest of the dark scene. These pixels are formally known as 'hot pixels' or 'warm pixels' and are often flagged and masked because they can retain and gain charge in unexpected ways. These pixels can arise from manufacturer defects or through degradation of the detector. Many new hot pixels have arisen in the lifetime of ACS/WFC (Avila 2017), the new hot pixels can be attributed to damages caused by high-energy particles. These hot pixels are created through either the depletion or diffusion processes which are generally created by interactions with high-energy particles. This has been produced in ground testing of CCDs, where different CCDs were placed at different positions from a radiation source and darks were taken (Belousov et al. 2012). The study showed a direct correlation between the number of hot pixels and proximity to the radiation source.

The orbit of HST is low enough that it passes through the Van Allen belts and crosses the South Atlantic Anomaly (SAA) seven to nine times a day (Rose et al. 2016). Since this is a region of space with very high levels of trapped particles, particularly protons with energies of 10 to 50 MeV (Sirianni et al. 2006). With each passage through this region, all of the instruments on board HST are exposed to damagingly high doses of high-energy particles. These high-energy particles, especially any protons, can damage silicon that comprises CCDs as they pass through the chip which can produce a vacancy in the silicon lattice that will allow electrons to pool. When particles interact with a semiconductor material, almost all the energy loss goes into ionization, which creates electron hole pairs. While more than 90% of these vacancies are healed, the remaining defects that are not can create new energy levels within the bandgap of the pixel allowing for extra charge to be persistent in the pixel (Hopkinson et al. 1996). This causes increased dark current from the extra charge traps that are generated from the degradation, and can make some pixels accumulate more electrons than others.

The overall dark rate and a significant portion of the number of hot pixels are often cured by a process called annealing (Riess 2002a). An anneal warms the detector from its controlled temperature setting for several hours then cools it back down to its operating temperature. This event happens approximately every 4

weeks on ACS depending on availability and schedulability of the telescope. We call the time between these events an anneal cycle, and it can change the entire dark scene including the overall dark current and hot pixels. Since thermally excited electrons largely generate the dark current, we expect the dark scene to change when the thermal state of the detector changes. Therefore, our analysis will be grouped by anneal cycles.

The signal from the individual pixels of the CCD can be stable or can evolve over time. This means that any given individual pixel may have unique characteristics that cannot be properly calibrated by simply subtracting the mean of several dark images over a small time cadence. Therefore, this paper documents our time series analysis of all dark images taken by the HST ACS/WFC to characterize the history of individual pixels over the lifetime of the detector. While we focus on ACS/WFC, this procedure can be used with any CCD on HST, and all code and methods presented here have been designed with that capability in mind.

### 1.3 Data processing

To properly and quickly analyze these darks, we created a new type of image. We rearranged the data so that the column dimension of the new image is the column of the original image and each row corresponds to time, so that the same pixel is repeated over and over creating a history of that column. In other words, the columns of a column image are the same column of an ACS/WFC dark image repeated with time increasing along the rows, this can be visualized in Figure 2. We call this a column image throughout this report because it contains the same column over and over throughout its history. Since CCDs are read out by passing current along the column to the serial register, building an image in this way is useful way analyze many different effects. We created column images for each of the 4096 columns of each of the two chips that comprise the WFC.

We also derived a new statistic and algorithm for measuring stability of a given pixel over an anneal period which we call the stability ratio (discussed further in Section 2.4). This new statistic can be used to inform pipelines and users of the variability of any pixel which can then be marked as unstable and updated in the data quality array of the products. While the ACS data pipeline does do checking for warm and hot pixels and marks them as such (Lim et al. 2012), it does not check for variability, which this new statistic and algorithm can facilitate.

## 2. Approach

### 2.1 Data Used

For this analysis, we used every full frame calibration dark image taken for ACS/WFC since 2002 up to the publishing of this document. This dataset contains 8,810 frames from 151 anneal periods used for the analysis which is every dark file used for superdark creation to 2017. We note that some darks taken immediately after an anneal cycle are discarded and not used in normal dark file creation as the detector is still achieving thermal equilibrium. The darks used are

taken with a relatively regular cadence and several at a time so that cosmic rays and other transient, non-calibration events can be properly screened out. With this extensive baseline, of calibration data we can characterize the individual pixels of the detector for the entire lifetime of the instrument.

### 2.2 Data Pre-processing

Significant preprocessing of the data is needed before making the column images. First, all images must be bias subtracted and overscan corrected. We are not trying to measure and the bias effects and overscan does not contribute to the overall dark current. Then all of the images are cleaned of cosmic rays. This is done with the CALACS software package (Lucas et al. 2016) using the default calibration settings for darks with two exceptions; first, that cosmic ray rejection was turned on and second, that we did not allow it to delete its intermediate files. we used the program ACSREJ (Lucas et al. 2016) to do the cosmic ray rejection on all of the darks over the entire anneal to ensure that our statistics are not skewed by extreme outliers caused by cosmic rays. Since the detector has significant CTE issues after its many years on orbit, especially in the dark images where the lowest background occurs (Anderson & Bedin 2010), the masks for the cosmic rays are grown by 3 pixels in all directions so that any flux from these transient features are discarded from our analysis. Pixels affected by cosmic rays are marked as *NaN* in the dataset so that they will not be included in any further analysis. This marking of *NaN* effectively creates a mask for these features so that later analysis may be performed if desired. The process creates temporary files called *blv* images. These are a byproduct of the CALACS (Lucas et al. 2016) pipeline and are bias subtracted, overscan corrected, cosmic ray rejected images that have all of the error arrays and data quality arrays correctly propagated.

It is worth noting for future studies that post flash was not removed from these data and may need to be removed depending on the type of analysis being performed. Other users of this dataset are encouraged to keep that in mind as they perform their analysis. The correct reference file to remove the post flash is also included in the attributes of the master column file, and example software for post flash removal is included in the software repository. These data have not been corrected using any CTE correction. At the time of this writing any version of the CTE correction does not correctly populate the error arrays with appropriate errors, which would make the analysis and statistic presented in Section 2.4 invalid.

### 2.3 New Data Storage Technique

This study is unique in its reconstruction of the original data sets into a more manageable and useful product. We create a new type of image that has the complete history of a column (and by extension, each pixel within that column) contained in a single image. This is done by stripping out the same column of each dark image and combining those columns into an image with time along the column axis. This is done for each column and each image for a given anneal

period. As discussed in Section 1.2, the anneal is the natural period over which to make these master column images since within the cycle the thermo-electric scene of the detector should be stable. This can also be seen in Figure 2 & Figure 4 and will be discussed in later sections. When the data are restructured, we utilize the HDF5 (The HDF Group 1997-2016) data framework to take advantage of its many features, including multiple concurrent reads of the same file, compact data format and easy tracking of metadata at the dataset, group and file levels. This allowed for many performance increases in our analysis, and is more convenient for storage and tracking all of the necessary metadata in logical places. Columns for both the science arrays and the error arrays are stacked in this data format for analysis.

It is also convenient to properly break up the images to get a homogenous dataset. This means that the images have to be split between chip and amplifier since several characteristics are different for each. Noise properties for each amplifier have been seen to be significantly different and evolve independently over time (Coe & Grogin 2014). Therefore, we break up the data by producing groups within the HDF5 hierarchy for each amplifier and putting the column datasets within that group for its amplifier. This allows for metadata associated with individual amplifiers to be easily recorded and retrieved and analysis of a specific amplifier to be performed much more easily. The datasets were also chunked in column major order (i.e. over the time axes), allowing for quicker time series analysis since time is now along the X-axis. The final structure of the files is 'Amplifier/columnNumber/type', where the type of data is stored as either 'sci' or 'err' for science or error arrays.

### 2.4 Variability Statistic

We have developed a statistic to evaluate the variability of each pixel using the column images. It is important to note that hereafter we refer to each row of the column image as a pixel, since each row represents with the same pixel of the ACS/WFC detector over time.

Since the images were run through CALACS, all of the errors that are present in the images have been correctly propagated into the error array (Lucas et al. 2016). Thus, we can assume that errors quoted in the error array is representative of the errors we expect to find in the image from Poisson noise. This error array includes accurately propagated Poissonian statistics for the noise contributed by the dark current for the non-CTE corrected images, as well as error propagation from the bias correction and read noise from the detector, and is kept in units of standard deviation. Since we can assume that we know what kind of errors to expect, and we have information about the pixel over the anneal cycle we can use the variance of the science array over that time scale and subtract the square of the mean of the error arrays. This gives us the difference of the actual dark variance from the expected normal Poissonian variance. We then ratio that to the expected variance which yields the stability ratio that we use to determine if a

pixel is stable. We add one to center the stability ratio around one instead of zero and make it easier to compare to an actual Poissonian distribution for verification.

**Equation 1 –** Stability ratio.

$$F = \frac{Variance(Science) - Mean(Error^2)}{Mean(Science)} + 1$$

Our algorithm was implemented with Python in a standalone script with a few accompanying sub modules also written in Python. These scripts take advantage of multiprocessing to compare the column images in the HDF5 format. This offered a very significant speed up of about 15x when compared to using astronomical standard FITs files since the HDF5 files allow multiple reads and reading in of a single dataset into memory at a time instead of reading the whole file.

### 2.5 Software

The Python programming language was used to perform data preprocessing and analysis with standalone programs, transforming raw dark images into column images. Several third party libraries were utilized, including Numpy (Jones et al. 2001-2016), which efficiently and easily handles the 2D arrays of pixels in a very efficient way, Astropy (Astropy Collaboration, 2013), which provides modules for easy I/O (Input/Output) of astronomical images into Numpy arrays and CALACS, which reduces raw ACS data (Lucas et al. 2016).

Our first step was to create the master column images. The master column image creation program essentially iterates over each full-frame dark image extracting the image, breaking up all of the columns and appending each column its own column dataset. This is done for both the science and error extensions of the image, which makes a total of 16,384 datasets for a given anneal (4,096 columns in each chip, 2 chips and 2 extensions) contains a variable number of darks depending on the length of the anneal. All of this is contained in an HDF5 file as described above. The program also keeps track of and appends the appropriate metadata associated with that dark to the attributes of the dataset, amplifier or file, while making sure that everything in the file is ordered by time for easier analysis. Thus, the resulting dataset contains the same pixels repeatedly in a time ordered fashion with all of the necessary metadata in the same order for a given anneal.

The types of metadata that are kept describe each column in the new column image, including the time and date that the exposure was taken as well as other data associated with the instrument and observing conditions at the time of observation. This allows for the easy relation of the column image to metadata associated with the telescope and could, with further analysis, uncover some interesting trends and relationships between the observatory overall and the effects

to an individual pixel. However, this paradigm is far beyond the scope of this investigation, we leave it for future work and only concentrate on variability here.

Once the column image is created and combined with its associated metadata, it allows for quick and easy time series analysis. This is because the actual pixel values of each pixel in that column for every dark ever taken are within a single image. Since the data is encapsulated within an HDF5 file that utilizes metadata and its hierarchical structure it can be easily adapted to multiprocessing as the data of interest is separated and multiple concurrent reads of the file are allowed. This means that an analysis of the data can be quickly and efficiently completed for a single anneal period. All analysis software products are implemented with this in mind; they all use multiprocessing for a speedup of several times over the serial analysis.

# 3. Results

### 3.1.1 Data Products

Figure 1 shows what a normal, full frame dark image looks like for a single chip of ACS/WFC. From this image, taken on October 22, 2015, we can see the dark current and how the hot pixels discussed above manifest themselves within a dark image. It can also be seen that the hot pixel trailing is more apparent farther from the readout due to CTE effects mentioned above. The red line in this image is the column that was stacked into the master column image in Figure 2 at the corresponding red line. Figure 2 shows what the data looks like when created as a column image in a way described in section 2.3; what is shown here is a composite of the all of the anneal period column images. Several conclusions can be made from a cursory visual inspection of this image. We see that the dark current changed multiple times (darker vertical bands) and that there are some pixels in this column that go hot and stay hot (persistently hot), while others blink on and off (unstably hot). These are the pixels we are trying to identify and mask. The master column image that is shown in Figure 2 shows the entire history of ACS, this is broken up for each anneal cycle in the HDF5 files which can be easily recombined to do lifetime analysis.

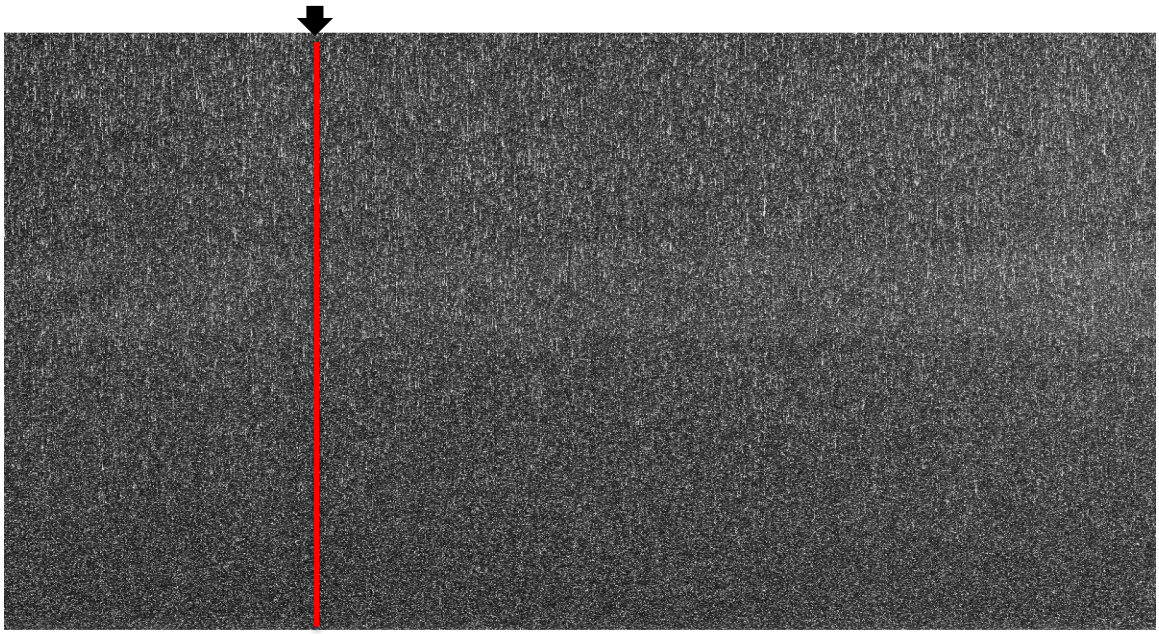

**Figure 1 –** Normal dark for ACS/WFC chip 2 from 10/22/15. Column 1040, indicated by the red line will be turned into one of the columns at the right side of Figure 2.

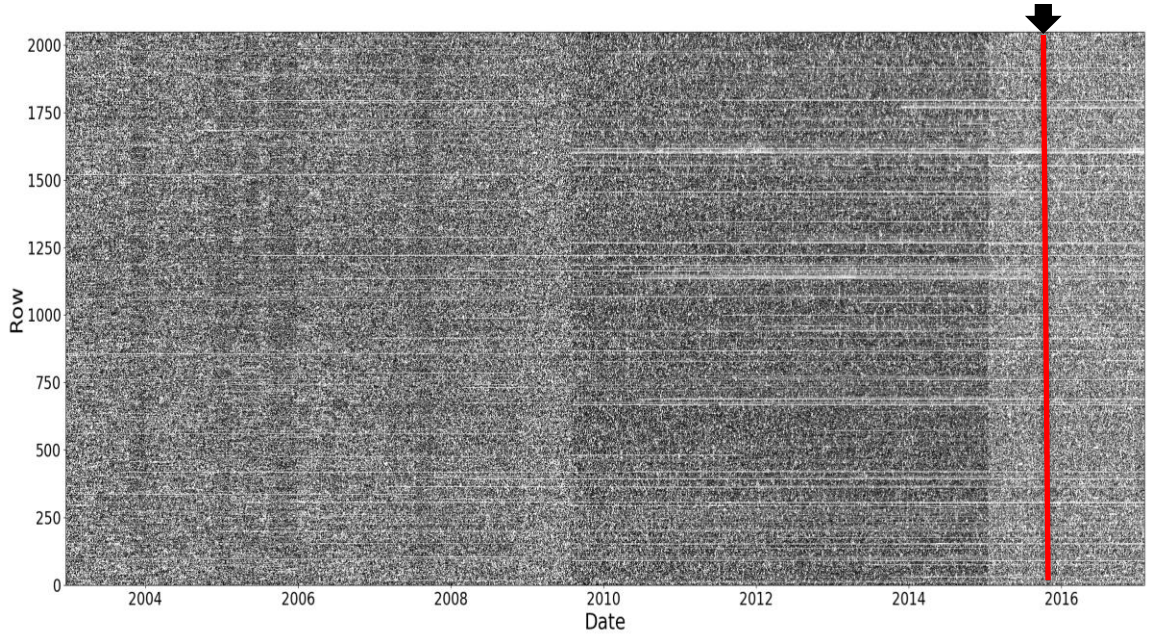


**Figure 2 –** Master Column image for Column 1040 of all ACS/WFC Darks from December 2002 onward. Since January, 2015 (Ogaz et al. 2015) the ACS team has been post flashing the normal Dark images which can be seen as an increase in intensity. This helps to mitigate the issue of CTE losses (Anderson & Bedin 2010) which allows us to get a more accurate estimate of the global dark current.

### 3.1.2 Other Calculations and Datasets

When we classify the pixels we also make several other potentially useful calculations save them in the HDF5 file as its own dataset so that they can be used again. We show the calculations that are saved in Table 1. *fratio* and *fmask* are calculated as described above where *fmask* is the mask of bad pixels found from the stability ratio. *scimean* and *errmean* are the mean values of the science and

error array values over that anneal. *nan_count* simply counts the number of NaN's that have been put into the sci and err dataset for that pixel. This includes both grown cosmic rays and decoding errors that are present in some datasets. The read noise is calculated as the mean of the square root of the error array squared, minus the science array. This is saved as the *readnoise* dataset. The standard deviation of the read noise calculation is also saved as the *rdstdev* dataset. While these other datasets are calculated, and may have very interesting results, they go beyond the scope of analysis of this document so are only mentioned here for reference.

**Table 1 -** Datasets saved in the HDF5 file. Example code for how to access and manipulate these datasets can be found in the *pixhist* git repository. The 4096 x 4096 array size only applies to ACS/WFC, it will be different for other detectors.

| Name | Description |
|---|---|
| Amp/col/sci | The master column dataset containing science array in format of '{amplifier}/{column_number}/sci' where amplifier is {'A', 'B', 'C', 'D'} |
| Amp/col/err | The master column dataset containing error array in format of '{amplifier}/{column_number}/err' where amplifier is {'A', 'B', 'C', 'D'} |
| fratio | 4096 x 4096 array of the calculated stability ratio for that anneal |
| fmask | 4096 x 4096 array of the calculated stability mask of bad pixels |
| scimean | 4096 x 4096 array of the calculated mean science values for that pixel in that anneal |
| errmean | 4096 x 4096 array of the calculated mean Error values in that pixel for that anneal |
| nan_count | 4096 x 4096 array of the calculated count of the number of NaN's that appear in that pixel for the entire anneal (either from cosmic ray or encoding error) |
| readnoise | 4096 x 4096 array of the calculated read noise in that pixel for that anneal |
| rdstdev | 4096 x 4096 array of the calculated Standard deviation of the calculated read noise |

### 3.2 Stability of Pixels

When we reduce all of this data look at each pixel individually as described above, we are able to classify pixels in four distinct ways. We define pixel stability by using a power function of the pixels' mean intensity relative to its *fratio* which is plotted in Figure 3 and is further discussed later. Using a power function in this way we are able to use the same classification methods for non-post-flashed darks as we do with post flashed darks because the signal of the hot pixels gives us enough signal to noise to determine its stability. Since post flashing the darks started in January 2015, we will be marking only hot pixels as stable or unstable before then. The coefficients used for the power function can be found in the

attributes of the *fratio* dataset. The classification is based on an individual pixel's stability and the traditional dark flagging threshold classification of hot and cold:

• **Hot Unstable**: Average flux greater than the hot pixel threshold and whose dark current value is varying by more than the allowed value.

• **Cold Unstable**: Low average flux and varying by more than allowed.

• **Hot Stable**: High average flux and stable throughout an anneal.

• **Cold Stable**: A good pixel with low average flux that is not significantly varying within in an anneal period.

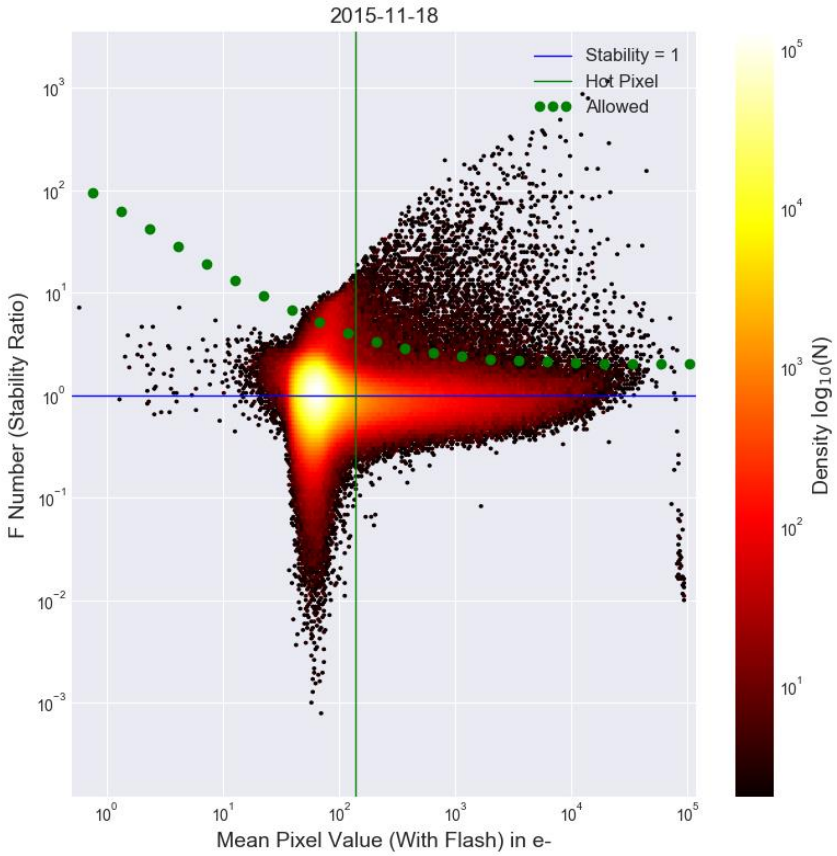


**Figure 3 –** Density plot of mean pixel intensity versus stability for the Nov 18, 2015 Anneal. Vertical green line is the hot pixel threshold. Horizontal blue line is a stability of 1. Dotted green line is the stability threshold, everything above will be marked unstable. Note: the axes and colormap are in log space. Mean pixel value is in total electrons in a 1000.5 second dark and includes flash.

Figure 3 shows a density plot of the dark intensity for each pixel over each dark versus that pixel's calculated stability ratio for the November 18, 2015 anneal period (same period as previous plots). As expected, the majority of the pixels are below the hot pixel and stability threshold and the majority of hot pixels are stable while many cold pixels that are not. We also see that extremely saturated pixels (far to the right) are calculated to be stable, but they should not be trusted as they go past normal pixel linearity. This is acceptable because they will be correctly marked as saturated in the dark DQ array and they will not contaminate user data.

The points with vert small measured stability that come down off the left side are mostly columns that are flagged as bias structure which have odd behavior in the darks as expected. We can also see that there are several stable pixels that have very low mean intensities which are likely sink pixels which are identified and corrected for in a different way (Ryon & Grogin, 2017) this may be another means to identify these pixels. Finally, it should be noted that this is the same anneal period as shown in Table 2. Figure 3 uses average dark values over the entire anneal for the hot pixel intensity where Table 2 uses a single super dark so the exact number of hot pixels will be different.

We show an example of the classification in Figure 4 where we plot an example of each of the four different kinds of pixels over the lifetime of the instrument and includes vertical dashed lines to indicate the anneal boundaries. From this plot it can be seen that some pixels' dark current can vary wildly within an anneal making reliable dark subtraction impossible. However, there are pixels that are traditionally marked as hot whose variance is low enough that it can be reliably dark subtracted. These are shown in the points in blue in Figure 4. This figure also shows that any pixel can go between these classifications for different anneal periods, i.e. annealing the detector 'cures' the extra flux (Riess 2002 a).

In order to classify each pixel and generate these plots, we flag every pixel whose stability ratio and intensity is greater than the evaluated power function as unstable. Figure 5 shows a histogram of the pixel stability ratio from Equation 1 calculated for every pixel for the November 2015 anneal. As expected, it is a roughly Poissonian distribution centered around 1.

Table 2 shows the statistics in the November 2015 anneal period and the Data Quality values for marking a pixel as hot or warm using the traditional thresholding method for the super dark 06u1504rj_drk.fits (useafter Nov 06 2015 00:12:34). The hot column of the table shows how many of the pixels in the super dark are marked as hot by using the simple threshold. Most of these hot pixels, which are generally discarded by users, are also in the Hot Stable column. The Hot Stable column indicates how many pixels that are marked as hot using the threshold but are stable using the method defined above. There are very few pixels that are hot and are unstable.

**Table 2 -** Statistics for superdark 06u1504rj_drk.fits (useafter = Nov 04 2015) compared to the stability ratio for that anneal. Hot is the total number of pixels that were marked hot in the superdark. Unstable is the total number of unstable pixels, both hot and cold. Hot Stable is the number of pixels that were marked as hot and are stable and Cold Unstable is the number of pixels that are cold and unstable.

| | **# Hot** | **# Unstable** | **# Hot Stable** | **# Hot Unstable** | **# Cold Unstable** |
|---|---|---|---|---|---|
| # pixels | 213999 | 20113 | 213742 | 257 | 19491 |
| % of detector | 1.27 % | 0.12 % | 1.27 % | 0.002 % | 0.12 % |

In Table 2, the unstable column is the total number of unstable pixels for this anneal period it includes pixels that are marked as either hot unstable or cold

unstable. The cold unstable column is for pixels that are below the hot pixel threshold and would normally be seen as "good" pixels, however using this method we see that they are too unstable to be trusted. In general, these unstable pixels should not be trusted regardless of their being hot or cold, as the amount of dark current contributed to this pixel is not properly measured by the normal darks and therefore cannot be corrected. This means that for an image taken on November 5, 2015, only 0.12% of the detector should be masked instead of the 1.27% hot pixel thresholding would remove. Even after 14 years on orbit the vast majority of the persistently hot pixels are stable within a given anneal period. This leads to the ability to reliably subtract the dark current from the science frame, resulting in an improved science image for all users.

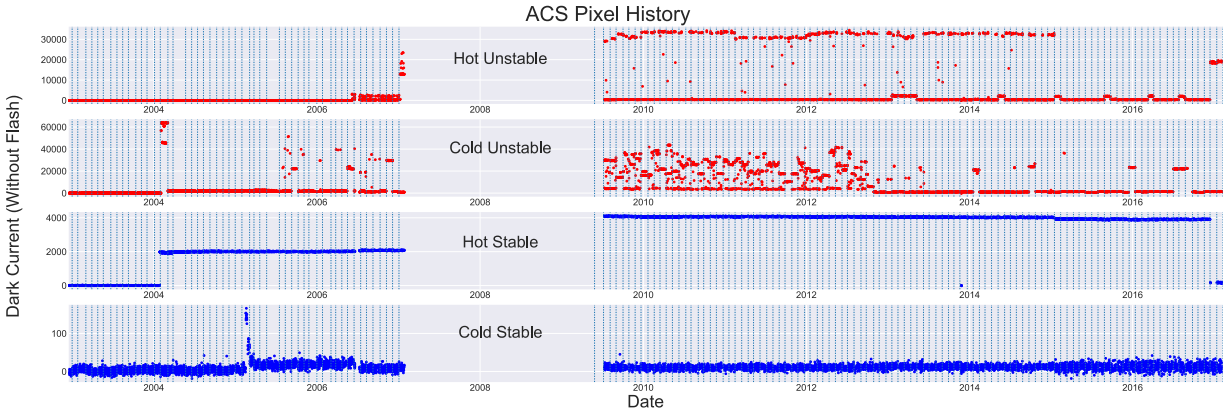


**Figure 4 –** The four different classifications of varying pixels from top to bottom over the lifetime of ACS. A pixel whose high average dark current (in electrons) makes it hot in the traditional sense but it varies from dark exposure to exposure making it unstable. Next is a pixel whose average low value would allow it to be traditionally marked as normal but it is varying significantly so it should not be trusted. Then a pixel that would be marked as bad, but its dark contribution is stable so it can be trusted. Finally, a normal, cold stable pixel. Vertical lines are anneal boundaries. The gap in the middle is when ACS was inoperable then revived by Servicing Mission 4. **Note that each plot is on a different scale**.

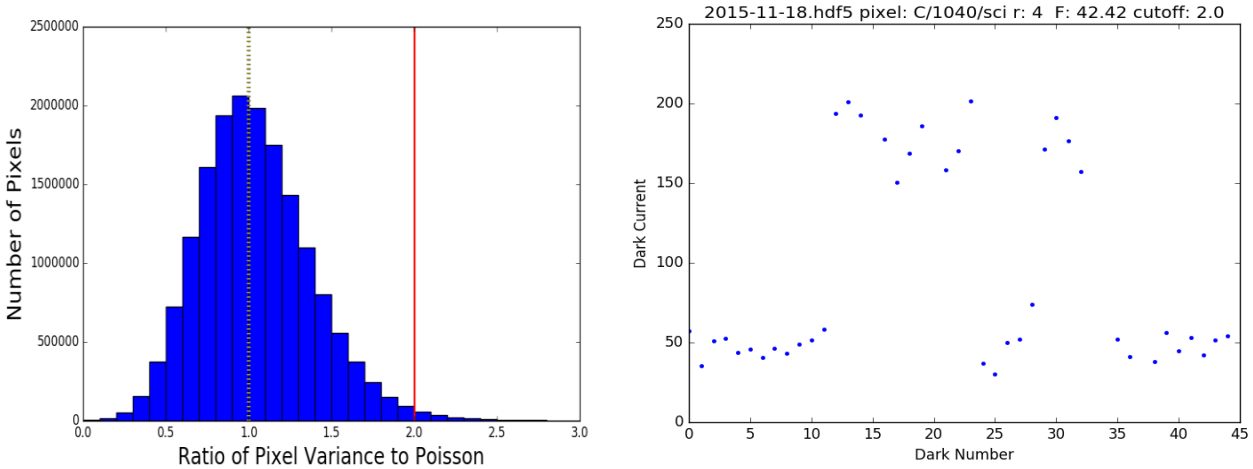


**Figure 5 – Left:** Histogram of the stability ratio of all of the pixels for the anneal in November 2015 (Same period as Table 2 and Figure 3) using Equation 1. **Right –** Dark current values of an individual, unstable cold pixel over the same anneal in electrons including post flash (Column 1040 (same as in Figure 2), Row 4). The variation makes it impossible to obtain an accurate measurement of its true dark current.

The right panel of Figure 5 demonstrates the reason for performing this kind of analysis. It shows the actual dark values for a given pixel over an anneal. proves that variability of this pixel makes it an unstable pixel. If one had a science image taken sometime between the dark number 12 and 13, one would not be able to have a good measurement of the dark current in this pixel. However, despite the unpredictable contribution from the dark current, this pixel would have been flagged as good in many of the super darks produced for the anneal. Due to the measured instability, users may want to reject this pixel depending on their science case. It will likely be too noisy for faint observations but if signal to noise is high enough it can be used, it is up to the user to decide.

Figure 6 illustrates the new stability metric for the lifetime of ACS/WFC. Despite the unpredictable contribution from the dark current, this pixel would have been flagged as good in many of the super darks produced for the anneal. From this we can conclude that the majority of the hot pixels are stably hot and will be reliably dark subtracted in science images to within their Poisson noise. It also shows that the majority of unstable pixels are below the hot pixel threshold. Users may not want to include them in their analysis depending on acceptable errors for their science.

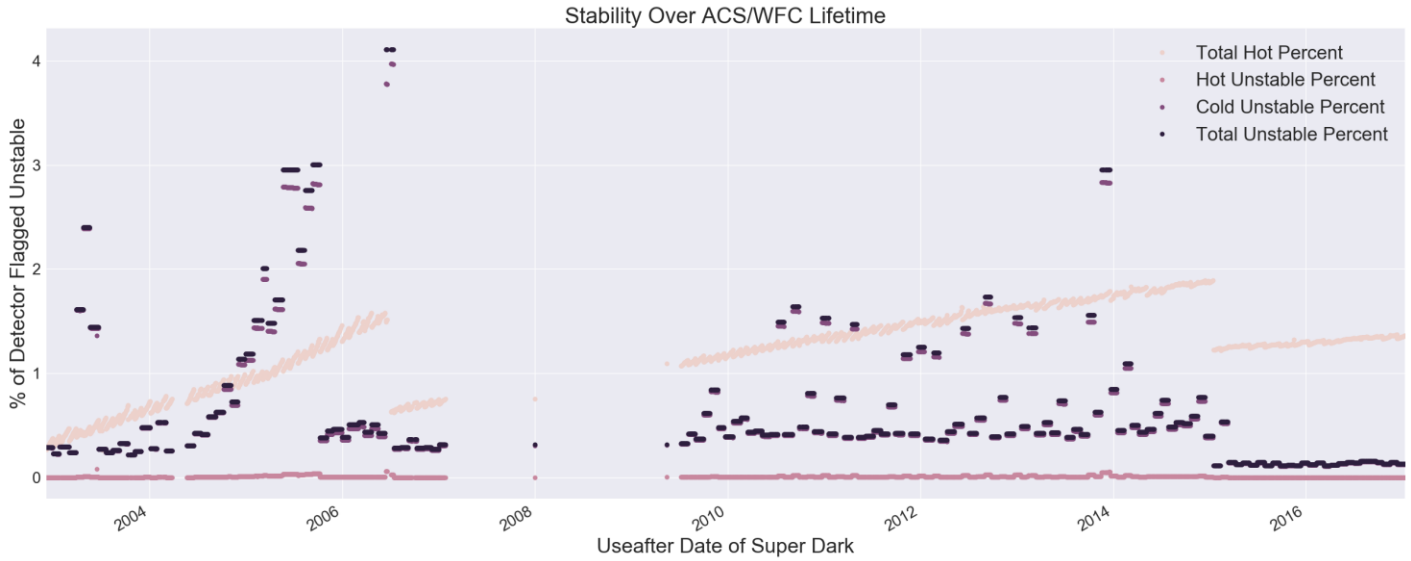


**Figure 6 –** Comparison of DQ arrays of all current super darks and stability over the lifetime of the instrument. X axes units are the date of useafter found in the header of the delivered super darks and Y axes units are percent of pixels flagged on the total detector (4096 x 4096 for ACS/WFC). The sharp decline in 2006 is due to the changing of operating temperature of the instrument. We will only be marking hot unstable before 2015 and all unstable after 2015 due to post flashing the darks starting in 2015 which causes the sharp decline in unstable pixels.

# 4. Implications

The incidence of hot pixels within any space-based CCD is expected to increase linearly with time. As ACS/WFC continues to function, the rate of hot pixels is expected to exceed the amount of incident cosmic rays in a 1,000 second

exposure (Sirianni et al. 2006). Since our average dark exposure time is 1000 seconds, this turns out to be a problem for properly calibrating the expected dark current because we need to have knowledge of the global and local dark current for accurate dark subtractions. Therefore, it becomes even more important to be able to mitigate the effects of hot pixel effects. The majority of the persistently hot pixels are stable relative to their expected errors, and all Poissonian errors are correctly propagated into the error arrays of each image, users may not want to discard the stable hot pixels depending on the acceptable errors for their science cases. Instead users should dark subtract these pixels and pay attention to the extra error that is contributed to the pixel value which is recorded in each error array of all ACS/WFC images. Using the information from the error array, users can make a more informed decision if they want to discard the hot pixels from their science data rather than blindly discarding all hot pixels.

As the detector continues to degrade, analysis of the dark images from more recent anneals becomes even more important. Table 2 shows statistics for the November 2015 anneal where the number of hot pixels is getting to be quite high. However, 99.8% of the hot pixels can be reliably corrected for and brought back into science analysis. This will reduce the likelihood that detector issues will compromise science products and help reduce the number of holes that appear in final drizzled products for observations with few or no dithers.

Dithering consists of taking multiple exposures of the target of interest and shifting each one by a few pixels. When the data is finally combined, the changed in position allows good measurements to fill in bad values and combat the effect of hot pixels. As the detector continues to degrade and the number of hot pixels continues to grow, it becomes more and more likely that a dithered hot pixel will shift to another hot pixel, leaving no data to fill in the gap. Therefore, this kind of correction becomes increasingly valuable as noisy data is better than no data at all.

Previously there was no information on the stability of an individual pixel. Users were only provided the hot and warm pixel flags based on thresholds provided by default in the darks (DQ values of 16 and 64 respectively). The unstable pixels will be marked in the DQ array of the super dark with a value of 32. Since the 32 DQ bit was previously unused, we can notify users that these pixels are unstable while preserving all other information that we previously provided the user including the current threshold flagging of warm and hot pixels. This allows users who want to maintain the old way of screening hot pixels from their data reduction to continue as they were but adds the ability to identify unstable pixels for users who wish to use every possible pixel for their analysis. Correspondingly, a new *MDRIZTAB* has been delivered to the Calibration Reference Data System (CRDS) that allows hot and warm pixels (DQ value of 16 and 64 respectively) to be included in final drizzled images but excludes these unstable pixels (DQ value of 32). This new *MDRIZTAB* will also be used by MAST to drizzle requested images and will contain all of the improvements from Hoffmann & Avila 2017. We believe that update should enhance the products that

users receive by default, especially when few frames are taken in a single visit. Users who wish to have drizzled data excluding hot and warm pixels as the pipeline currently operates will need to re-drizzle their images and change the *astrodirzzle* 'dqbits' keyword to exclude them from the final drizzled products.

We show results of using the new darks and *MDRIZTAB* together in Figure 7, which shows a zoomed in region of jdba1s010_drc.fits (Figure 8). This program only has two exposures per visit and the default drizzled products using the old flagging still contains cosmic rays (circled in red) where they coincide with hot pixels in one of the two images as the hot pixels have been screened out from the creation of the final image and were filled in with the cosmic ray. Using the new pixel flagging, the hot pixel is kept, reliably subtracted, and that value is used to fill the gap. Using the new reference files, these cosmic rays are more likely to be identified and screened out from observations with only two visits.

There is very little difference in the noise properties between the drizzled images using the two different sets of darks. Table 3 shows the mean and standard deviation from 5 different locations across the drizzled image which are marked in Figure 8. These statistics are performed over a 200x200 pixel square aperture at each location outlined in Figure 8 and show very little difference between the two different combinations as one would expect if the hot pixels were correctly subtracted. Since this association only has 2 exposures, any difference between the two like a single very hot pixel that was not corrected for would show up especially in the regions where there is only background.

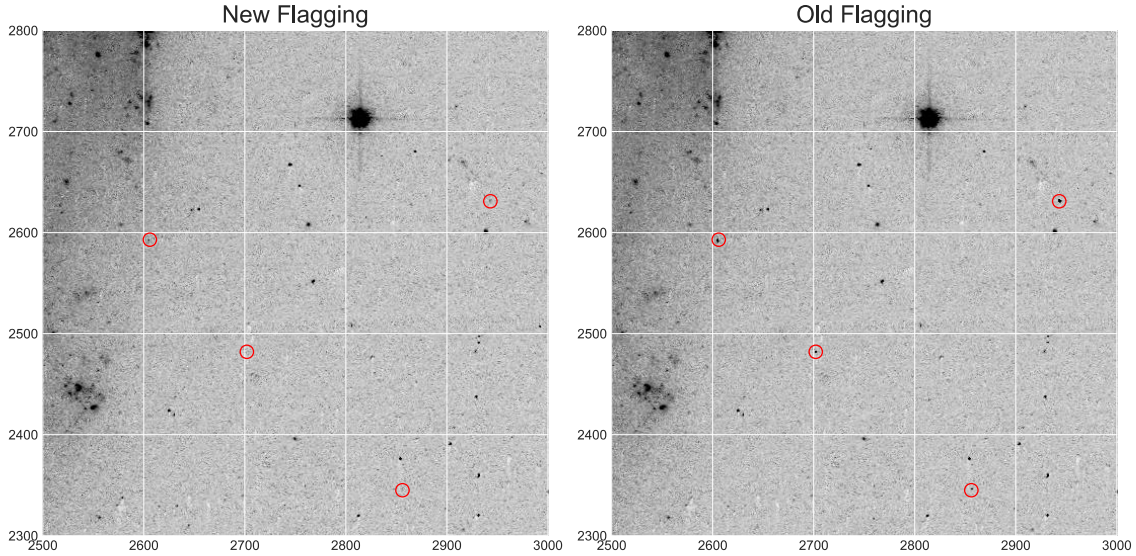


**Figure 7** – Zoomed in region of jdba1s010_drc (in Figure 8) same dark on both panels but the left is reduced with the stability flags in the DQ array and the new MDRIZTAB while the right uses the old method. Red circles indicate cosmic rays that were properly identified using the new darks and new MDRIZTAB. Units are in X and Y pixels.

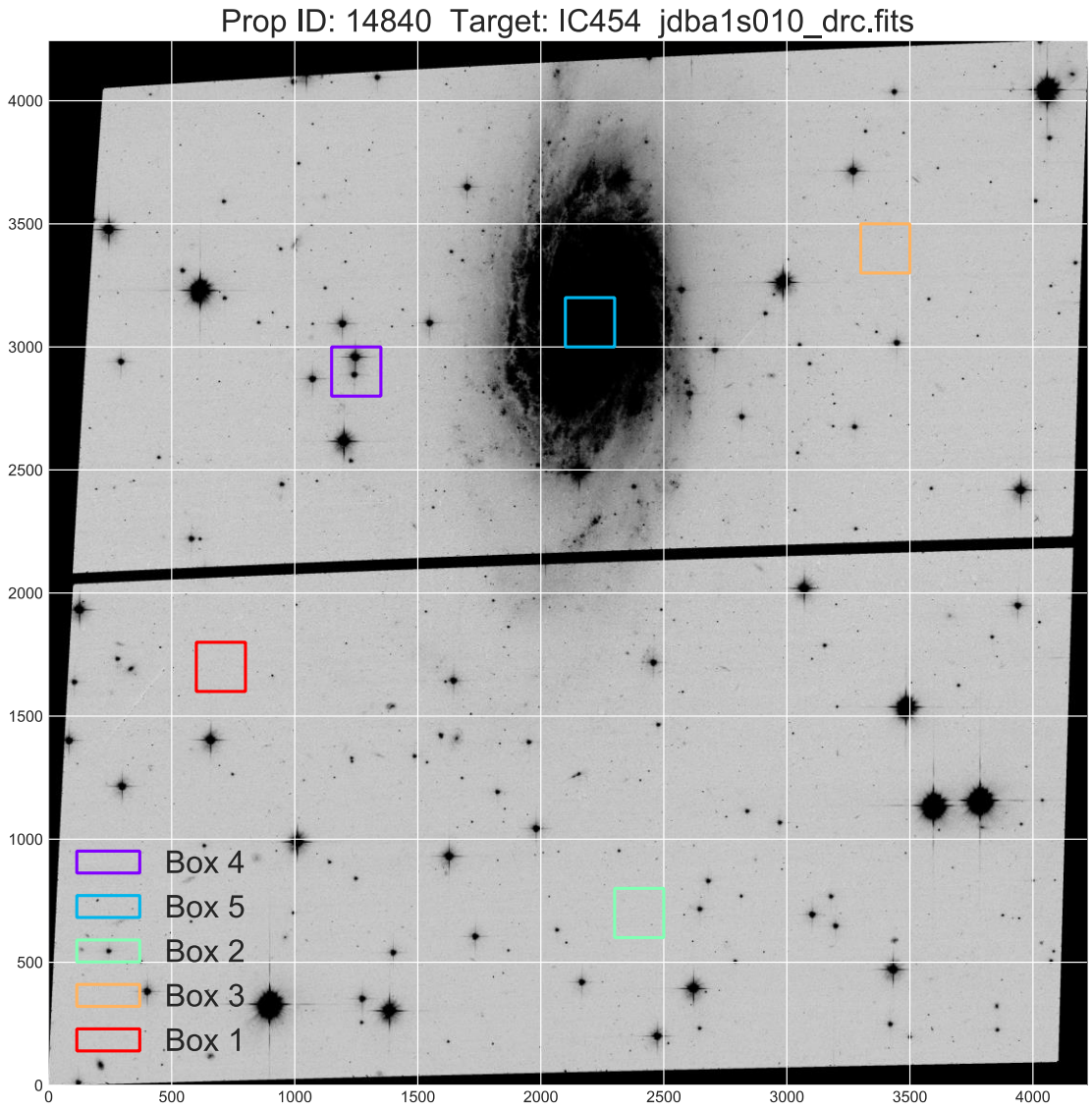


**Figure 8 -** jdba1s010_drc.fits from proposal 14840 target IC454. Only two observations are taken on this association. Boxes correspond to box number in Table 3. Units are in X and Y pixels.

**Table 3** Statistics for 200x200 pixel boxes on drizzled images whose locations are outlined on Figure 8 reduced with new dark DQ flagging and old dark DQ flagging.

| | Mean of Box (e-/sec) | | | Standard Deviation of Box | | |
|---|---|---|---|---|---|---|
| | **New** | **Old** | **Difference** | **New** | **Old** | **Difference** |
| **Box 1** | -0.0012 | -0.0016 | 0.0004 | 0.0167 | 0.0162 | 0.0005 |
| **Box 2** | -0.0010 | -0.0012 | 0.0002 | 0.0143 | 0.0141 | 0.0002 |
| **Box 3** | 0.0016 | 0.0016 | 0.0000 | 0.0144 | 0.0282 | -0.0138 |
| **Box 4** | 0.2528 | 0.2527 | 0.0001 | 6.2004 | 6.1905 | 0.0099 |
| **Box 5** | 0.9175 | 0.9173 | 0.0001 | 0.6864 | 0.6866 | -0.0002 |

As of this report, the dark pipeline (Lim et al. 2012) has been updated to produce the data products described here automatically and mark new darks with the instability flag of 32. All new darks produced for ACS/WFC will have this information provided which will be propagated into the science images by CALACS. All old darks will be reprocessed and this new stability information will be included.

# 5. Discussion on Previous Dark Studies

A time series analysis of darks has been performed for another space based CCD, the PICARD-SODISM mission (Hochedez et al. 2014). While we arrange the data for analysis in a similar way, we approached the analysis in different ways and with different goals in mind. Here our goal is to determine stability of a given pixel within an anneal period, whereas the goal in Hochedez, et al. 2014 was to create a model for the dark current. Since ACS regularly anneals the CCDs and the PICARD-SODISM does not, we would be unable to do that kind of modeling of the overall dark current. However, their use of the Unbalanced Harr Transform or their implementations of the Box-Cox power transform (Fryzlewicz 2007) may be applicable to ACS/WFC and may be very useful way to analyze this data. Since forward modeling is not the intent of this analysis, it will be left for future work.

Unfortunately, an analysis of dark images at the level of individual pixels has never been performed for instruments on HST or other space or ground based cameras that we have been able to find. There are many papers that discuss and characterize the overall dark current for every HST CCD, especially ACS/WFC (Coe & Grogin 2014, Mutchler et al. 2004, Riess 2002 a & b, Cox et al. 2003), WFC3/UVIS (Bourque & Baggett 2016, Biretta & Bourque 2014) and even ACS/SBC which is a MAMA detector (Cox 2004, Avila, 2017). None look in-depth at each pixel individually. Some ACS/WFC dark characterizations are as recent as 2015 (Ogaz et al. 2015) and some just after the launch of the instrument in 2002 (Riess et al. 2002 a & b) but we could find none that look at each hot pixel individually for any instrument. Many papers mention that there appear to be persistently hot pixels and notice that they can be ‘healed’ or notice this transient behavior but do not seek to try to correct them (Riess 2002 b, Sirianni et al. 2006).

As discussed before, this kind of analysis on the ground is complicated because it is likely that at the end of the night, many ground based CCDs are turned off, are allowed to warm, or may have electrical current fluctuations that may affect the dark scene when not in use. This variation in temperature and basic detector properties can change the thermal properties of the camera, thus it will change the dark scene too often and make a long time series analysis invalid. Luckily, HST is somewhat unique because the instruments are kept at a constant temperature and electrical current (with the previously discussed exception for annealing) so the scene in the dark current does not change significantly. As such, there have been many recent attempts to understand the dark images overall from

all CCDs on HST (WFC3 CCDs, SBC Darks). These previous attempts to understand the detector have yielded interesting results and at times even try to study their time variability, but none of them analyze each individual pixel in a similar way as we do combined with time variability.

Very early analysis of the ACS/WFC dark images noticed the existence of persistently hot pixels and based on the first 7 months of data projected that the growth of these anomalous pixels could make up as much as 6% of the detector, i.e. 1 out of every 16 pixels by 2010 (Riess et al. 2002 b). This early analysis also suggests that the noise in these persistently hot pixels is greater than Poisson, so users should dither rather than trust a normal dark subtraction. This report goes on to suggest that users should dither their observations to avoid these hot pixels. If the degradation continues at that rate dithering will not be sufficient for avoiding these pixels as the number of persistently hot pixels is expected to grow linearly with time (Riess 2003). However, due to new super dark creation techniques now in use (Ogaz et al. 2015), we have enough measurements to say if a pixel is stable to within their Poisson noise.

We were unable to find any further analysis into these persistently hot pixels for ACS/WFC, however the Space Telescope Imaging Spectrograph (STIS) performed an early analysis of their persistently hot pixels and found that the number of persistently hot pixels to be relatively stable over time (Hayes et al. 1998). This finding was also later confirmed after a decade more data had been taken (Wolfe et al. 2009). These reports only state that the number of occurrences of persistently hot pixels seem to be stable but does not characterize their noise properties or seek to correct or perform any further analysis on them.

# 6. Conclusions

Issues in dark current can affect detectors in unusual and unexpected ways, so calibration of the dark current must progress as each instrument continues to function. In this paper, we present a successful analysis of each of the 16 million pixels of the ACS/WFC CCD using every dark image taken over the entire history of the instrument. This resulted in useful classifications that can better inform users about the validity of their data so that they no longer have to discard every hot pixel from their images. While this saves a small percentage of the total detector, it will prevent many scientists from needlessly discarding valuable data and prevent the inclusion of cosmic rays in some cases. The measurements of stability presented here will be implemented in the ACS/WFC dark images in the coming months along with other major changes to the ACS/WFC reductions.

Users should now be able to trust the dark subtraction of stable hot and warm pixels in most cases. However, users should pay attention to the extra Poisson noise contributed by these pixels and make a judgement for themselves as to include these pixels or not based on their intended science.

## Acknowledgements

The authors would like to thank the entire ACS team and Katie Salazar for their comments on this report that greatly enhanced its readability.

## References

Anderson, J., & Bedin, L. 2010, PASP, 122, 1035

Astropy Collaboration, Robitaille, T. P., Tollerud, E. J., et al. 2013, AAP, 558, A33

Avila, R., et al. 2017, "ACS Instrument Handbook", Version 16.0 (Baltimore: STScI).

Avila, R., 2017, Updated Measurements of ACS/SBC Dark Rates, Tech rep., Space Telescope Science Institute, ACS ISR 2017-04

Belousov, A., Mustafin, E., & Ensinger, W. 2012, Journal of Instrumentation, 7, C11002

Biretta, J., & Bourque, M. 2014, WFC3 Cycle 19 and 20 Dark Calibration: Part I, Tech. rep., Space Telescope Science Institute, WFC3 ISR 2014-04

Bourque, M., & Baggett, S. 2016, WFC3/UVIS Dark Calibration: Monitoring Results and Improvements to Dark Reference Files, Tech. rep., Space Telescope Science Institute, WFC3 ISR 2016-08

Coe, D., & Grogin, N. 2014, Readout Dark: Dark Current Accumulation During ACS/WFC Readout, Tech. rep., Space Telescope Science Institute, ACS ISR 2014-02

Cox, C. 2004, SBC Dark and Cumulative Images, Tech. rep., Space Telescope Science Institute, ACS ISR 204-14

Cox, C., Mutchler, M., & van Orsow, D. 2003, Elevated Temperature measurements of Hot Pixels, Tech. rep., Space Telescope Science Institute, ACS ISR 2004-04

Fryzlewicz, P. 2007, Journal of the American Statistical Association, 102, 1318

Golimowski, D., Cheng, E., Loose, M., et al. 2011, ACS after Servicing Mission 4: The WFC Optimization Campaign, Tech. rep., Space Telescope Science Institute, ACS ISR 2011-04

Hayes, J. E., J., Christensen, J. A., & Goudfrooij, P. 1998, STIS CCD Anneals, Tech. rep., Space Telescope Science Institute, STIS ISR 1998-06

"HDF5"; The HDF Group. 1997-2016, Hierarchical Data Format, version 5

Hochedez, J.-F., Timmermans, C., Hauchecorne, A., & Meftah, M. 2014, AAP, 561, A17

Hoffmann, S., & Avila, R., 2017, Updated MDRIZTAB Parameters for ACS/WFC, Tech. rep., Space Telescope Science Institute, ACS ISR 2017-02

Hopkinson, G. R., Dale, C. J., & Marshall, P. W. 1996, IEEE Transactions on Nuclear Science, 43, 614

Jones, E., Oliphant, T., Peterson, P., et al. 2001-2016, SciPy: Open source scientific tools for Python, [Online; accessed 2016-11-28]

Lim, P. L., Ogaz, S., Armstrong, A., et al. 2012, Bias and Dark Calibration of ACS/WFC Data: Post-SM4 Automated Pipeline, Tech. rep., Space Telescope Science Institute, ACS TIR 2012-01

Lucas, R., et al. 2016, Advanced Camera for Surveys Data Handbook v. 8.0 (STScI)

Mutchler, M., Sirianni, M., van Orsow, D., & Riess, A. 2004, Bias and dark calibration of ACS data, Tech. rep., Space Telescope Science Institute, ACS ISR 2004-07

Ogaz, S., Anderson, J., & Golimowski, D. 2015, Post-Flash Calibration Darks for the Advanced Camera for Surveys Wide Field Channel (ACS/WFC), Tech. rep., Space Telescope Science Institute, ACS ISR 2015-03

Riess, A. 2002, The Projected Growth of Hot Pixels on ACS WFC, Tech. rep., Space Telescope Science Institute, ACS ISR 2002-09

Riess, A., Mutchler, M., & van Orsow, D. 2002, A First Look at Hot Pixels on ACS, Tech. rep., Space Telescope Science Institute, ACS ISR 2002-06

Riess, A. 2003, in HST Calibration Workshop: Hubble after the Installation of the ACS and the NICMOS Cooling System, ed. S. Arribas, A. Koekemoer, & B. Whitmore, 47

Rose, S., et al. 2016, Hubble Space Telescope Primer for Cycle 24 (STScI)

Ryon, J., Grogin, N., 2017, Sink Pixels in ACS/WFC, Tech. rep., Space Telescope Science Institute, ACS ISR 2017-01

Sirianni, M., Mutchler, M., & Lucas, R. A. 2006, in the 2005 HST Calibration Workshop: Hubble After the Transition to Two-Gyro Mode, ed. A. M. Koekemoer, P. Goudfrooij, & L. L. Dressel, 45

Widenhorn, R., Blouke, M. M., Weber, A., Rest, A., & Bodegom, E. 2002, Vol. 4669, Sensors and Camera Systems for Scientific, Industrial, and Digital Photography Applications III, ed. M. M. Blouke, J. Canosa, & N. Sampat, 193–201

Wolfe, M. A., Davies, J., Proffitt, C., Goudfrooij, P., & Diaz, R. 2009, STIS CCD Anneal Results, Tech. rep., Space Telescope Science Institute, STIS ISR 209-01